Quaternary Science Reviews 212 (2019) 187–198

Contents lists available at ScienceDirect

Quaternary Science Reviews

journal homepage: www.elsevier.com/locate/quascirev

Volcanic eruption eye-witnessed and recorded by prehistoric humans

İnan Ulusoy [a, *], M. Akif Sarıkaya [b], Axel K. Schmitt [c], Erdal Şen [a], Martin Danišík [d], Erdal Gümüş [e]

[a] Hacettepe University, Department of Geological Engineering, 06800, Beytepe, Ankara, Turkey
[b] Istanbul Technical University, Eurasia Institute of Earth Sciences, 34469, Sarıyer, Istanbul, Turkey
[c] Institut für Geowissenschaften, Universität Heidelberg, Im Neuenheimer Feld 234-236, 69120, Heidelberg, Germany
[d] John de Laeter Centre, TIGeR, Curtin University, GPO Box U1987, Perth, WA, 6845, Australia
[e] Manisa Celal Bayar University, Geopark Research Center & Demirci Vocational School, Department of GIS, 45900, Demirci, Manisa, Turkey

ARTICLE INFO

Article history:
Received 30 October 2018
Received in revised form
19 March 2019
Accepted 26 March 2019

Keywords:
Western Turkey
Anatolia
UNESCO global geopark
Salihli
Petrographs
Human footprints
Rock painting

ABSTRACT

Human footprints in hydrovolcanic ash near Çakallar volcano (Kula, Western Turkey) were discovered in 1968. A nearby pictograph interpreted as depicting Çakallar volcano would define it as the oldest site where humans demonstrably eye-witnessed a volcanic eruption and possibly artistically recorded it. Despite Çakallar's volcanological and cultural importance, its eruption age has remained controversial. Here, two independent dating methods, cosmogenic ^{36}Cl and combined U-Pb and (U-Th)/He zircon (ZDD) geochronology, yielded the first internally consistent eruption ages controlled by detailed volcanostratigraphic mapping. Concordant ^{36}Cl ages of 4.7 ± 0.6 ka (errors 1σ) were obtained for a cone-breaching lava flow. ZDD ages for crustal xenoliths from scoria deposits directly overlying the footprints yielded an age of 4.7 ± 0.7 ka. This firmly places the Çakallar eruption and prehistoric human footprints, and plausibly the rock art, into the Bronze Age, reinforcing the notion that prehistoric artwork recorded natural events.

© 2019 Elsevier Ltd. All rights reserved.

1. Introduction

Hominid footprints are rare trace fossils providing unique constraints on human evolution and prehistory. Worldwide, about 18% of all documented hominid footprints are preserved on surfaces of volcanogenic deposits (Lockley et al., 2008). These ichnofossils have revealed important details about human presence and societal resilience in regions prone to volcanic disasters. During construction of the Demirköprü dam near Sindel village (Salihli district, Manisa, Turkey; Fig. 1) in the 1960's, workers excavating scoria from one of Kula's volcanoes noticed human footprints, which were exceptionally well preserved in fine-grained volcanic ash (Barnaby, 1975; Yalçınlar, 1987; Kayan, 1992). These footprints, which are now widely known as the "Kula footprints", occur in a beige colored ~6 cm thick hydrovolcanic (phreatomagmatic) ash layer (Fig. 2) deposited onto an erosional surface of gneissic country rock. The ash was immediately buried by scoria, thus preserving the footprints. Depths of human footprints reach up to ~3 cm, and displacement bulges around their margins protrude at centimeter-scales, indicating that the ash was wet and coherent (e.g., Marty et al., 2009, Fig. 2). Lateral dimensions are 27 cm from toe to heel and 10 cm wide (as measured by us for the Hacettepe University specimen; Fig. 2a), but different foot sizes indicating multiple individuals have been identified (Tekkaya, 1976; Yalçınlar, 1987). Small prints potentially indicate the use of staffs, and *Canis* species traces exist alongside human footprints (Yalçınlar, 1987; Akdeniz, 2011).

Approximately 2 km from the footprint site, a pictograph in a sheltered location between gneissic boulders (Fig. 3a) has long been known by local villagers as Kanlıtaş (*bloody rock*), but was only recently described in the scientific literature after reports emerged in the internet (Akal et al., 2009; Akdeniz, 2011). It was interpreted to depict the erupting Çakallar cone (Akdeniz, 2011). Enhanced images of the painting reveal an upwards narrowing cone with a circle drawn on its top with several dots inside flanked by two subvertical lines (Fig. 3). A thick line of about the same length as the cone is drawn near its bottom. Three hand marks without thumb and forefinger are located above the cone (Fig. 3). Because of unequivocal evidence from the footprints that humans witnessed a

* Corresponding author.
E-mail address: inan@hacettepe.edu.tr (İ. Ulusoy).

https://doi.org/10.1016/j.quascirev.2019.03.030
0277-3791/© 2019 Elsevier Ltd. All rights reserved.

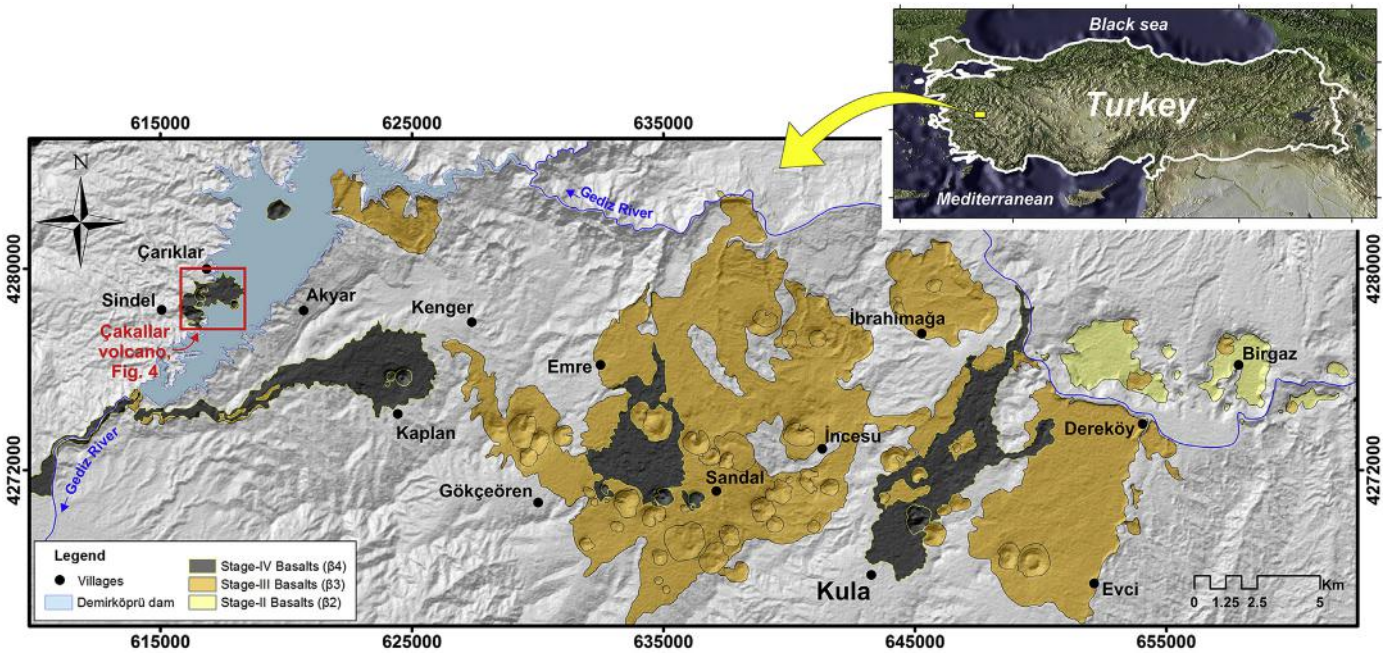

Fig. 1. Location of the Kula Volcanic Field. Map showing basaltic cover from older to younger effusive stages over hillshade topography (ALOS PALSAR Digital Elevation Model - © JAXA/METI, 2006 derived - ASF DAAC, 2016) based on the geological map of Şen (2002) and Şen et al. (2014). Hillshade illumination is from the southeast. Coord. Sys. UTM, datum: ED1950. Inset shows the study location within Anatolia. Inset satellite image is a MODIS Global Composite (NASA, 2008). (For interpretation of the references to color in this figure legend, the reader is referred to the Web version of this article.)

volcanic eruption, this pictograph is uniquely significant among several prehistoric art pieces interpreted to illustrate an erupting volcano (e.g., Mellaart, 1964; Karakhanian et al., 2002; Nomade et al., 2016).

Discovery of the Kula footprints triggered frequent attempts to determine their age, starting immediately after the footprints were first unearthed. However, in addition to the difficulties of dating young basalts, these earlier dating attempts generally lacked detailed mapping to place geochronological data into a stratigraphic context. To amend this, we established a firm volcanostratigraphy and integrated it with newly generated radiometric ages using two independent state-of-the-art methods for dating young volcanic rocks, combined U-Pb and (U-Th)/He zircon geochronology (ZDD; zircon double-dating) and cosmogenic ^{36}Cl dating. Although it is obvious that U-Pb zircon dating of volcanically-heated basement xenoliths cannot reveal eruption ages due to the slow diffusion of Pb in zircon, we show that Pb-mobilization from the outermost crystal rims occurred during pyrometamorphism. This aids in the interpretation of (U-Th)/He zircon ages.

1.1. Geological evolution of the Çakallar volcanism

The Kula volcanic field in western Anatolia is a Quaternary basaltic volcanic field with remarkably well exposed youthful volcanic structures. The 'Burned Lands' of Kula (*Katakekaumene* according to Strabo; a famous Greek geographer, philosopher, and historian who lived in Anatolia during 64 or 63 BC to c. AD 24; Radt, 2004), based on their geologic and cultural importance, were designated a United Nations Educational, Scientific and Cultural Organization (UNESCO) Geopark in 2013. Çakallar volcano, ichnofossils and Kanlıtaş paintings are Earth heritage monuments of international importance and are recognized as Geosite by the UNESCO to be protected and promoted due to their outstanding scientific, educational and aesthetic value (Gumus, 2014).

Previous work has subdivided the volcanic evolution of the Kula volcanic field into three explosive (Strombolian) and effusive eruptive stages: β2 (ca. 2 - 1 Ma), β3 (ca. 300–50 ka) and the most recent, β4 (<25 ka; Fig. 1; Hamilton and Strickland, 1841; Washington, 1893; Erinç, 1970; Bunbury et al., 2001; Westaway et al., 2004, 2006). Because of the youthfulness of Çakallar volcano (stage β4), it is reasonably assumed that the pre-eruptive surface morphology and geology was very similar to today's, which consists of eroded gneiss boulders and surfaces with alluvial channel-fill and terraces. Drainage channels typically cut into bedrock, which is partly covered by soil with up to decimeter-scale thickness. Our mapping indicates that Çakallar volcanism started with a hydrovolcanic eruption producing an ash layer covering an area of approximately 1 km radius (Fig. 4). The hydrovolcanic ash layer directly mantles the topography and covers pre-volcanic gneiss and soil surfaces (Fig. 5a and b). The thickness of the ash layer ranges from 40 cm in proximal outcrops (Fig. 5c) to 1 cm at distal locations, with footprints being located within the ash layer where it is 1–7 cm thick (Fig. 2). The isopach map (Fig. 6) illustrates that the thickness of the ash layer increases southeast of Çakallar cone with a likely eruption center located in the south-central part of a small ridge, which is now a peninsula in the modern Demirköprü dam lake. In proximal locations with thicknesses >20 cm, the ash layer is normally graded with accretionary lapilli in the lower levels grading upwards into ash (Fig. 5c). In proximal and medial outcrops, the upper levels of the ash are generally laminated (Fig. 5a, c), probably indicating pulsating eruption bursts. In a groundmass composed of glass shards, the ash contains fresh clinopyroxene, plagioclase, amphibole, and olivine similar to those of β3 and β4 basalts of Kula. Xenocrysts of quartz, muscovite and rare sapphirine derived from the metamorphic basement are minor components.

Soon after the emplacement of the hydrovolcanic ash, construction of scoria cones began in the order of C0, C1, C2, C3 and C4 (Figs. 4, 5d and 6), suggesting that the vent system changed to drier

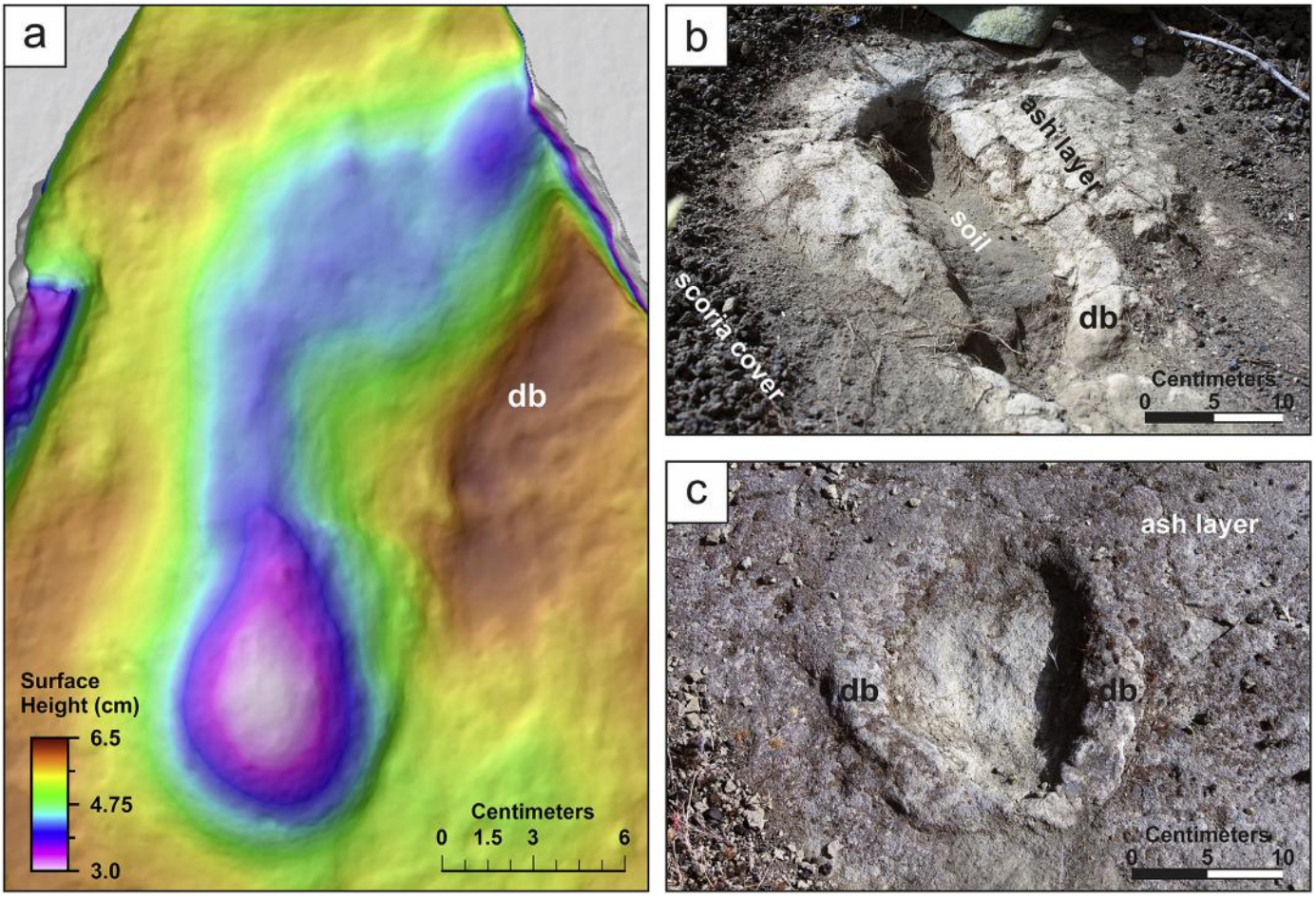

Fig. 2. Kula footprints on the hydrovolcanic (phreatomagmatic) ash layer. a) Digital surface model derived from the footprint track sample using the Structure from Motion/Multi-view Stereo-photogrammetry (SfM-MVS) method, b) in-situ footprint within thin (<3 cm) ash layer, with the print penetrating into the underlying soil layer, c) unidentified track, possibly partial footprint or animal trace. Displacement bulges (db) around the footprints due to the pressure applied on the wet ash are indicated. (For interpretation of the references to color in this figure legend, the reader is referred to the Web version of this article.)

conditions. The broad alignment of these cones (Fig. 4) is in accordance with the NW-SE directed main faults and lineaments in the Kula basaltic volcanic field and the southern graben system (Erinç, 1970; Şen et al., 2014). Contacts between the ash layer and overlying basaltic scoria are always sharp without reworking (Fig. 5a and b), indicating continuous eruptive emplacement. The tallest of the five scoria cones is Çakallar (C2) (Fig. 5d), which is the source for extensive scoria deposits (dark gray in geological map: Fig. 4) in addition to coarse (1–1.5 m) bombs/blocks with sag-structures in proximal locations. Its eastern rim was breached during construction by basaltic lava flowing eastward from the crater (Figs. 4 and 5d). The lava flow is massive, roughly columnar jointed in its lower reaches, and more vesicular, brecciated, and aa-like towards the top (Fig. 5e). A thin scoria cover is locally preserved on the aa-like surface of lava flows (Fig. 5f), indicating synchronous Strombolian and effusive activity. The lower flanks of C1 are locally overlain by proximal deposits of Çakallar cone (C2) whereas cone C3 is built on the northern rim of Çakallar cone, and overlies its deposits locally. Strombolian activity ended with four small spatter cones (C4) scattered mostly to the E and NE of Çakallar (Fig. 4) with C3 and C4 Strombolian deposits overlying the lava flow. The easternmost scoria cone C0 is older than C2 because the lava onlaps onto C0 scoria deposits (Figs. 4 and 5g).

The emplacement of Çakallar cones and lava modified the local drainage patterns and caused damming of the Kolcu and Değirmen streams (Fig. 4) to the W and NW of Çakallar where alluvial deposits formed (Kayan, 1992; this study). Değirmen stream was subsequently diverted northward where it locally breached the scoria deposits prior to its confluence with the Kolcu stream. Kolcu stream follows the northern edge of the lava flow until it enters the modern Demirköprü dam lake, which now fills the alluvial plain of the Gediz River. Regarding the pre-eruptive morphology and the generally W-E drainage pattern of Gediz River tributaries, it is plausible that both Kolcu and Değirmen streams once drained into wetlands where Çakallar cone erupted (Figs. 4 and 6). This might have contributed to the initial hydrovolcanic eruption.

2. Methods

2.1. Previous ages and new dating methodology

The earliest age assessment of Çakallar volcanism shortly after discovery of the footprints was based on regional terrace geomorphology and yielded an age of ca. 250 ka (Ozansoy, 1968). Therefore, earlier researchers misinterpreted the tracks as footprints of *Homo neanderthalensis*. However, correlations between Anatolian and European Pleistocene terraces were erroneous, and following careful geomorphological observations and geological mapping, the age of Çakallar volcanism was revised to between ca. 10 and 2 ka (Erinç, 1970). Sanver (1968) determined that the

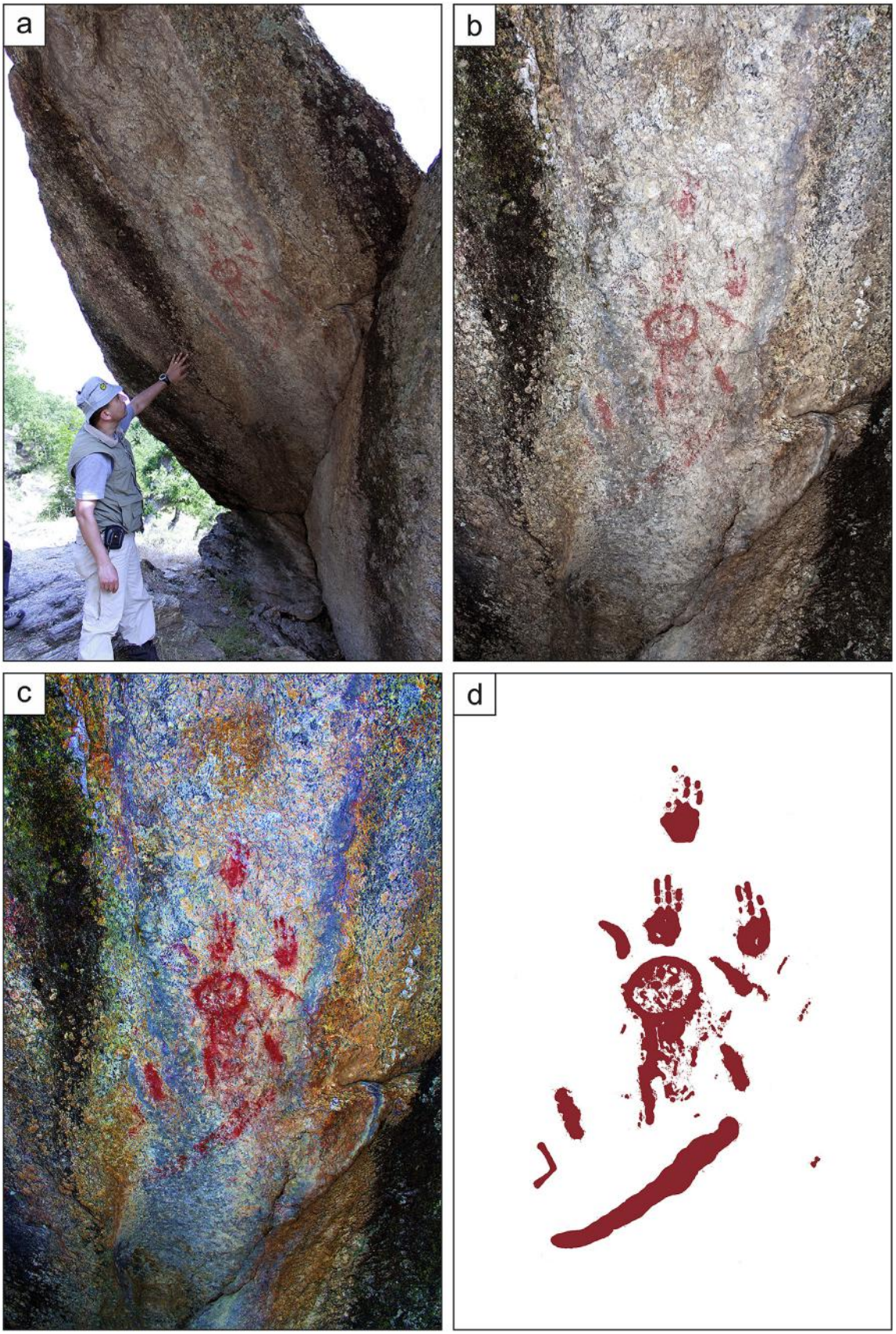

Fig. 3. Kanlıtaş rock pictograph near Çakallar volcano. a) Rock shelter and the painting on the downward sloping rock face with volcanologist nearby, b) direct view of the rock painting in true color, c) color-enhanced version of the rock painting generated by saturation stretch. The enhanced image clarifies the cone shaped feature, the lower elongated thick line, the three-fingered handmarks and other details, d) reconstructed version of the painting for clarification. (For interpretation of the references to color in this figure legend, the reader is referred to the Web version of this article.)

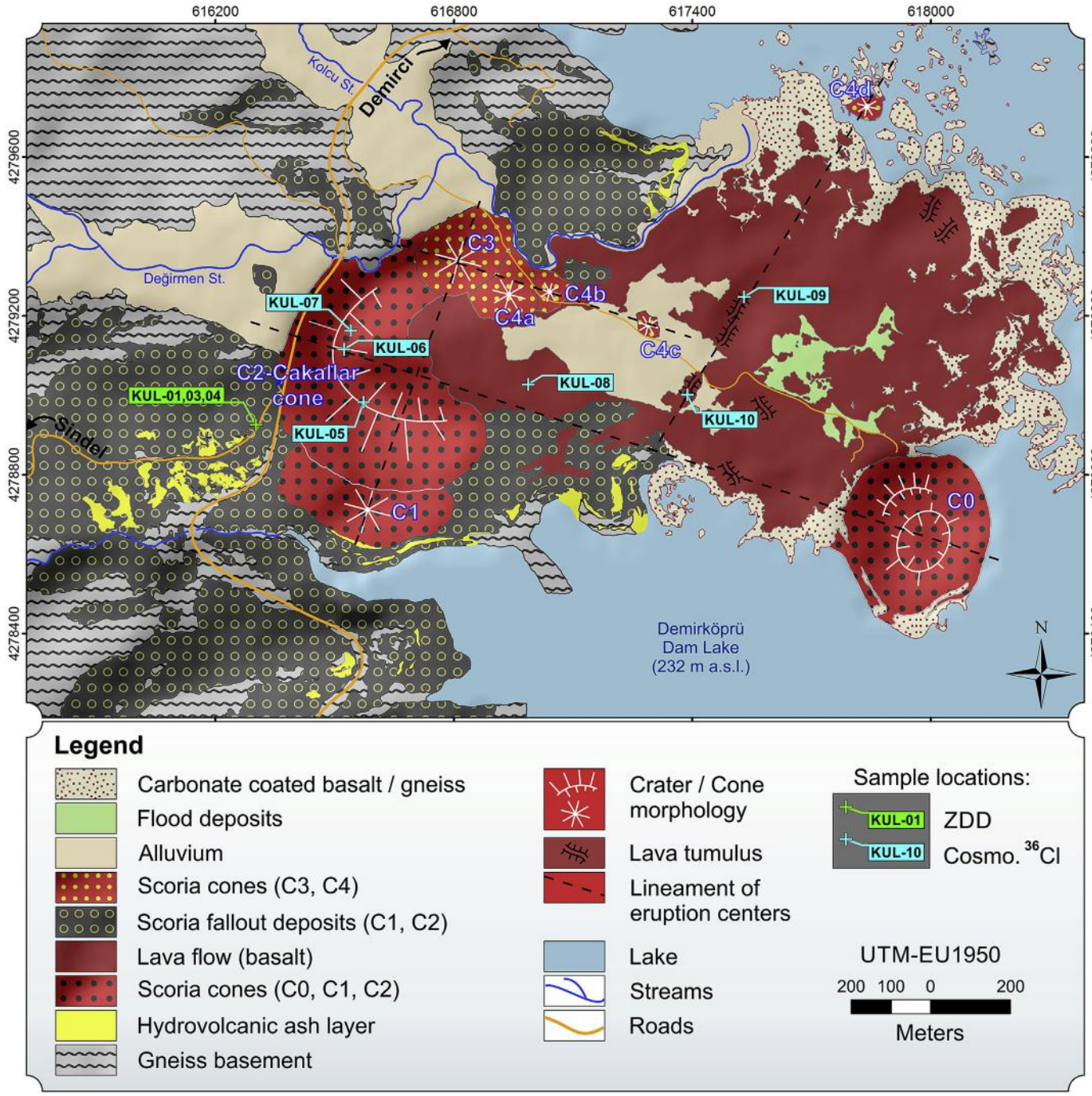

Fig. 4. Detailed geological map of the Çakallar volcano on the modern peninsula in Demirköprü dam lake. Sample locations are indicated on the map. Coord. Sys. UTM, datum: EU1950. Background topography is an ALOS PALSAR Digital Elevation Model (© JAXA/METI, 2006 - ASF DAAC, 2016) derived hillshade. (For interpretation of the references to color in this figure legend, the reader is referred to the Web version of this article.)

youngest basaltic scoria cones and lava flows at Kula are geomagnetically normal and thus broadly of Late Pleistocene-Holocene age (cf. Tekkaya, 1976). Based on these dates and a careful study of footprint morphology, consensus emerged that the footprints belong to *Homo sapiens* (Yalçınlar, 1987; Kayan, 1992; Tekkaya, 1976). Thermoluminescence dating of the Çakallar volcanic sequence yielded dates of 65.0 ± 7.8 ka (bottom of ash layer), 49.0 ± 4.8 ka (hornblende from the top of the ash layer), and 26.0 ± 5.2 ka (scoria above the ash layer) (Göksu, 1977, 1980). Although seemingly stratigraphically consistent, the ca. 16 ka age difference between top and bottom of a single, thin hydrovolcanic ash layer is implausible in terms of eruption dynamics (Kayan, 1992; Heineke et al., 2016; Westaway et al., 2004). Recently, Heineke et al. (2016) targeted a metasedimentary block on top of Çakallar scoria cone for cosmogenic ^{10}Be dating and determined an exposure age of 11.2 ± 1.1 ka. Intriguingly, they report even younger ages for other 'stage β4' volcanoes at Kula (Heineke et al., 2016).

Here, we place new radiometric age determinations into a volcano-stratigraphic context based on detailed geological mapping (Fig. 4). This includes isopach mapping of the ash layer hosting

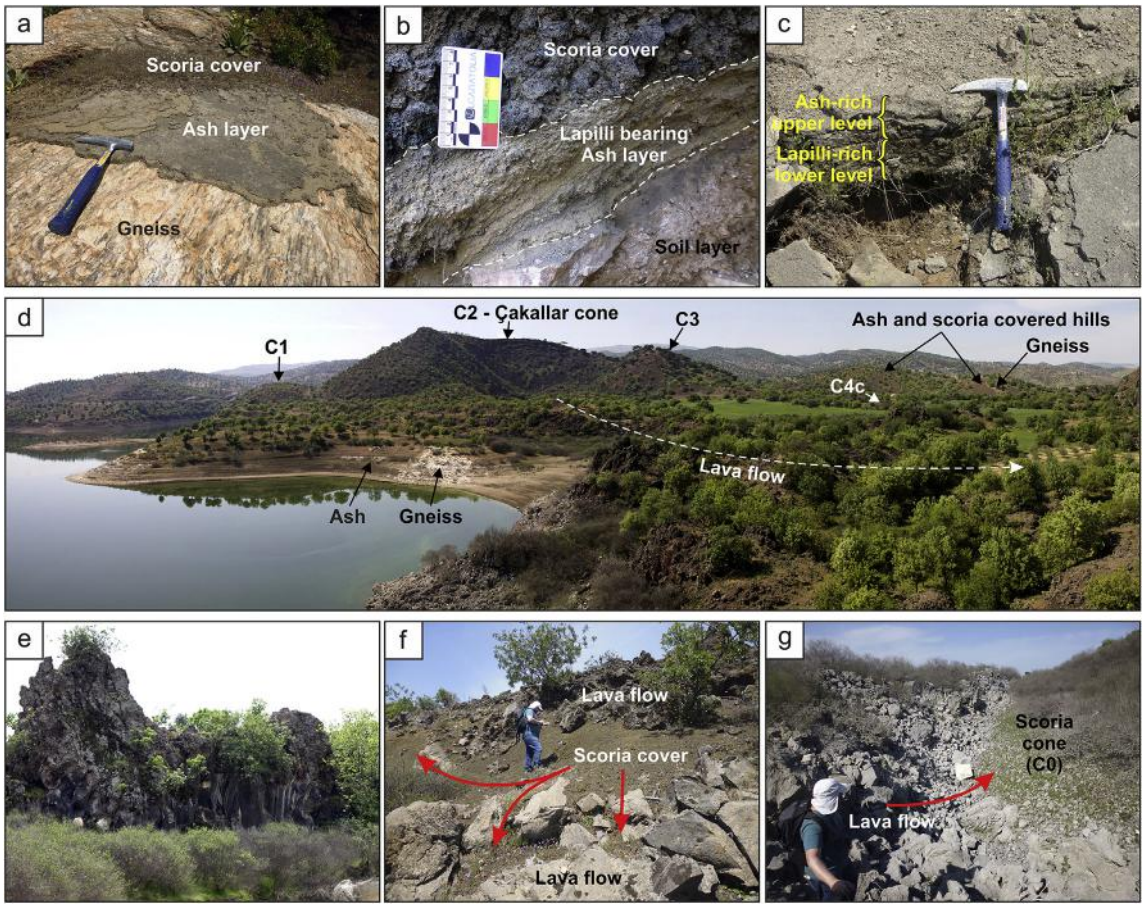

Fig. 5. Field pictures of Çakallar volcano. a) laminated ash layer at medial distance from the vent deposited onto gneiss surface and overlain by loose scoria deposits, b) lapilli-bearing ash directly underlying scoria of the main Çakallar cone, c) proximal ash deposit with normal grading from lapilli to ash and laminated upper layers, d) overview of the Çakallar cone, smaller cones and the lava flow in the south central part of the peninsula, e) northern edge of the cone-breaching basaltic lava flow with a massive, roughly columnar jointed lower part and vesicular, aa-like upper part, f) scoria cover on the breaching lava surface, g) the same lava flow onlapping on scoria cone C0.

the footprints to locate the eruption center of the hydrovolcanic activity.

Six samples were dated using the cosmogenic ^{36}Cl surface exposure dating method, providing the time-span that the rock samples were exposed to cosmic radiation on the surface. Three of them are from proximal crater-rim agglutinates, which comprise volcanic bombs/blocks and scoria ejected from the crater (Fig. 4: KUL-05, KUL-06 and KUL-07). This is also the location where Heineke et al. (2016) collected a metasedimentary block from the same pyroclastic agglutinate deposit. Three other samples for surface exposure dating were collected from the lava flow extending eastward from the breached Çakallar scoria cone (Fig. 4: KUL-08, KUL-09 and KUL-10).

Three gneissic xenoliths for zircon geochronology were collected from distal scoria fallout deposits which directly cover the ash layer in close proximity of the footprint site southwest of the main Çakallar cone (Fig. 4: KUL-01, KUL-03 and KUL-04). These ~5–10 cm (in diameter) xenoliths are friable with a glassy matrix, which provides evidence for partial melting in contact with the basaltic magma. They also preserve weak banding, indicating a gneissic protolith consistent with local basement outcrops. Zircon crystals extracted from the xenoliths were dated by the ZDD method (Danišík et al., 2017a) in order to determine the age of eruption. This approach assumes that the (U-Th)/He system in the xenolithic zircons was completely reset (i.e., experienced protracted temperatures of >180–200 °C, Reiners et al., 2004) during the eruption. In addition, a sample of local stream sediment (13T13; courtesy R. Hetzel), which unlike the xenoliths was not affected by volcanic heating, was analyzed for comparison because it provides a broad overview of zircon ages from the regional basement rocks that are the source for the xenoliths.

2.2. Determination of ^{36}Cl surface exposure ages

Surface exposure ages represent the end of scoria cone/lava emplacement, and thus the timing of volcanic activity. The top few cm of crater rim agglutinate and lava were removed using hammer and chisel to obtain 400–500 g sample. Sample preparation for exposure dating was conducted at Istanbul Technical University according to the procedures described in Sarıkaya (2009). Rock samples were crushed and ground to the size fraction of 0.25–1 mm. The samples were leached with dilute nitric acid (10%) to remove any meteoric chlorine and any secondary carbonates present, then chlorine was liberated from the rock matrix by dissolving the sample (~5 g) in a mixture of hydrofluoric and nitric acids in pressure digestion vessels (Parr #4748) at 130 °C for 6 h. ^{35}Cl (99.7%) enriched Aldrich carrier was added to the samples and chlorine was precipitated by adding $AgNO_3$. Sulfur (including any ^{36}S) was removed from the samples by repeated precipitation as $BaSO_4$. The Cl isotope ratios were measured at ASTER AMS, France.

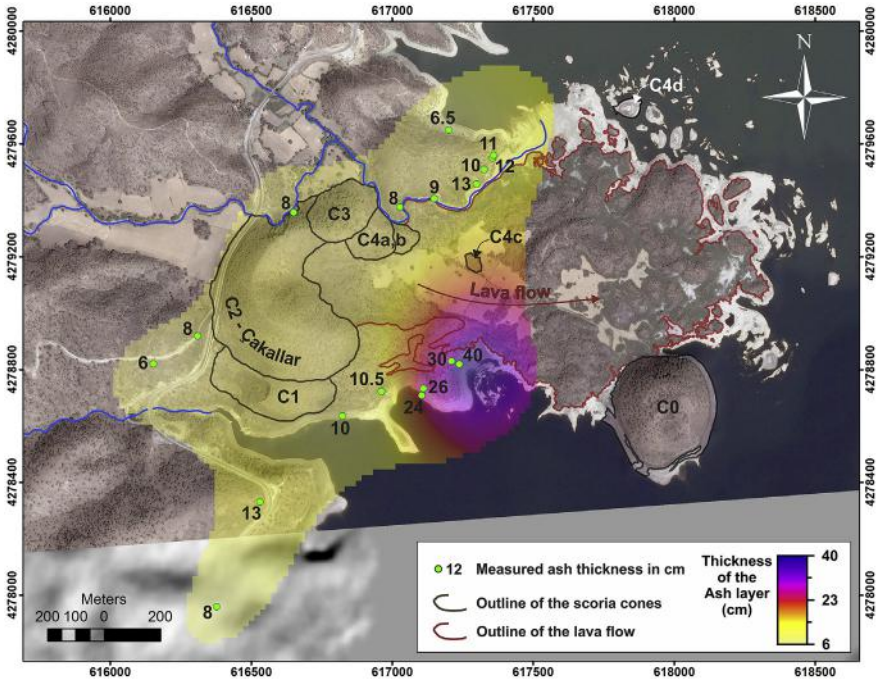

Fig. 6. Isopach map of Çakallar hydrovolcanic ash layer. Numbers indicate corresponding ash thickness in centimeters. Background Google Earth imagery (Map data: Google, CNES/Airbus image, imagery date: 21 August 2016 - image courtesy of Google Earth™ mapping service, ©2017 Google LLC, used with permission. Google and the Google logo are registered trademarks of Google LLC.) draped over ALOS PALSAR Digital Elevation Model (© JAXA/METI, 2006 - ASF DAAC, 2016) derived hillshade image. Coord. Sys. UTM, datum: ED1950. (For interpretation of the references to color in this figure legend, the reader is referred to the Web version of this article.)

Table 1
Cosmogenic ^{36}Cl and combined U-Pb and (U-Th)/He zircon geochronology results, sample locations and properties.

	Sample ID	Latitude (WGS84)	Longitude (WGS84)	GPS Elevation	Landform / Sample	Sample thickness	Rock density	Topographic shielding factor	Surface exposure ages: Without erosion correction	Surface exposure ages: Erosion corrected (5 mm ka^{-1})
		°N (DD)	°E (DD)	(m)		(cm)	(g cm^{-3})		(ka)	(ka)
Cosmogenic ^{36}Cl	KUL-05	38.65019	28.33906	376	C2 crater rim	8	2.6	1	7.9 ± 1.1	7.5 ± 1.0
	KUL-06	38.65132	28.33881	369	C2 crater rim	6	2.6	1	4.9 ± 1.0	4.7 ± 1.0
	KUL-07	38.65174	28.33910	383	C2 crater rim	5	3	1	11.4 ± 2.1	10.6 ± 1.9
	KUL-08	38.65049	28.34384	257	lava flow	4	2.6	0.9974	4.1 ± 0.9	3.9 ± 0.9
	KUL-09	38.65242	28.35011	247	lava flow	5	2.6	0.9996	5.6 ± 1.2	5.3 ± 1.1
	KUL-10	38.65020	28.34844	245	lava flow	7	2.6	0.9998	5.7 ± 1.2	5.4 ± 1.2

	Sample ID	Latitude (WGS84)	Longitude (WGS84)	GPS Elevation	Landform / Sample	Single crystal (U-Th)/He ages range	Number of grains	MSWD	(U-Th)/He age, weighted average
		°N (DD)	°E (DD)	(m)		(ka)			(ka)
ZDD	KUL-01	38.65002	28.33607	302	Xenolith from distal scoria fallout	3.8 - 51.2	16	n.a.	n.a.
	KUL-03					5.2 - 360.7	18	n.a.	n.a.
	KUL-04					3.4 - 10.9	10	0.3	4.7 ± 0.7

n.a. = not applicable because of incomplete degassing.
MSWD = mean square weighted deviation.
ZDD = combined U-Pb and (U-Th)/He zircon geochronology (zircon double-dating).

A laboratory-blank correction was also applied. Major and trace elements were measured at Activation Laboratories, Inc., Canada (Supplementary Table 1). Rock densities were measured by gravimetric methods at the Hacettepe University.

Cosmogenic ^{36}Cl production rates (Marrero et al., 2016) [56.3 ± 4.6 atoms ^{36}Cl (g Ca)$^{-1}$ a^{-1} for Ca spallation, 153 ± 12 atoms ^{36}Cl (g K)$^{-1}$ a^{-1} for K spallation, 13 ± 3 atoms ^{36}Cl (g Ti)$^{-1}$ a^{-1} for Ti spallation, 1.9 ± 0.2 atoms ^{36}Cl (g Fe)$^{-1}$ a^{-1} for Fe spallation and 743 ± 179 neutrons (g air)$^{-1}$ a^{-1}] were scaled following the time-dependent Lifton-Sato-Dunai method (the so-called "LSD" or "SF" scaling, Lifton et al., 2014). Production due to thermal neutron capture of ^{35}Cl is responsible for 70–80% production of ^{36}Cl in the samples, with lesser contributions from spallation and negative muon capture by ^{40}Ca (8–14%) and by ^{39}K (10–13%). In-situ ^{36}Cl is also produced as a result of the capture by ^{35}Cl of low-energy neutrons which are generated during the decay of U and Th (non-cosmogenic). The nucleogenic ^{36}Cl production (1.0–1.4% of total production) is calculated according to Fabryka-Martin (1988).

Topographic shielding corrections were made by taking inclination measurements of the horizon at each sample location in 45°

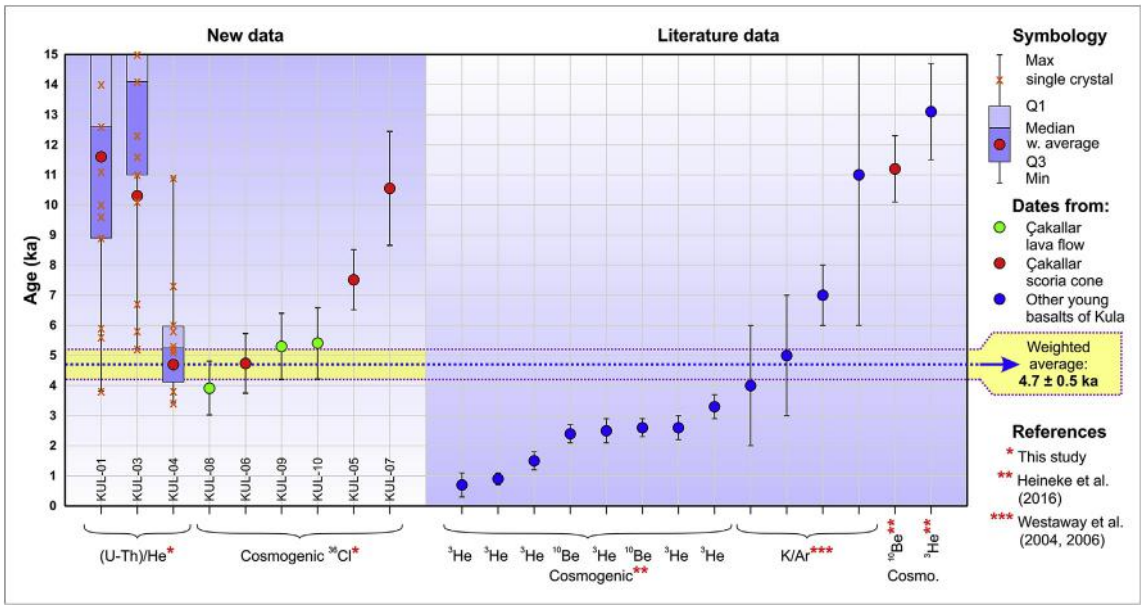

Fig. 7. Radiometric ages of Çakallar volcano. (U-Th)/He zircon and cosmogenic ^{36}Cl geochronology of Çakallar volcano (left side; this study) and literature data for Kula stage β4 basalts in ranked order (right side). Red and green circles represent all radiometric results obtained for Çakallar volcanism in the literature (excluding Göksu, 1977, 1980; see text); blue circles represent other β4 scoria cones and lava flows (i.e. Kula, Sandal, and Kaplan villages; Fig. 1). Weighted average of cosmogenic ^{36}Cl (KUL-08, 09, 10) and replicate (U-Th)/He zircon ages from pyrometamorphic metesedimentary xenolith KUL-04 is shown as horizontal bar (4.7 ± 0.5 ka). Error bar symbols for (U-Th)/He ages are indicated in the legend. (For interpretation of the references to color in this figure legend, the reader is referred to the Web version of this article.)

increments from the north using a hand-held inclinometer and compass, and also by measurements of the surface dip angle (Gosse and Phillips, 2001). Snow corrections were not applied to our samples due to the climactic condition of the region and the low elevation of the sample sites. According to the Meteorological Survey of Turkey, the number of snow-covered days in the study area was about 4 days between 1970 and 2017. We assume a similar climate regime for the Middle Holocene as today (Robinson et al., 2006), as δ^{18}O and δ^{13}C values for Lake Gölhisar (200 km south of the study area) indicate generally drier conditions for the second half of the Holocene than in the period before 5.1 ka (Eastwood et al., 2007). Furthermore, during the Late Holocene (1.5 ± 1.0 ka ago), Jones et al. (2007) reported that precipitation totals in Eski Acıgöl (central Turkey) approached modern values with deviations ranging between 12% wetter and 13% drier than today. Moreover, as a sampling strategy, we preferred to sample from the highest flat surfaces on the crater rim and lava flows where snow accumulation is mitigated by wind exposure. The MS Excel spreadsheet of Schimmelpfennig et al. (2009) was used to calculate exposure ages. Correction on nucleogenic ^{36}Cl disequilibrium conditions resulting from Cl degassing during eruption were made using a hypothetical crystallization age (5 ± 1 ka) of the minerals. Assuming a crystallization age of 10–50 ka would make ages younger by 1.1%–11.5%, which is within stated uncertainties. An erosion correction of 5 mm ka^{-1} was assumed for bedrock weathering due to the low-grade erosional features at the rock surface (few mm to 5 cm). All essential information to reproduce resultant cosmogenic ages is presented in Table 1 and Supplementary Table 1.

2.3. Combined U-Pb and (U-Th)/He zircon (ZDD) geochronology

Zircon was separated from crushed xenoliths using standard density and magnetic separation protocols. In addition, detrital zircon crystals were extracted from modern stream sediment derived from regional basement rocks using the same techniques. Secondary Ionization Mass Spectrometry (SIMS) analyses of pristine zircon crystal surfaces were carried out to determine U-Pb crystallization ages, and possible disturbances of parent-daughter relations in the U decay system for the same crystals used in subsequent (U-Th)/He analysis. For this, hand-picked zircon crystals were pressed into indium metal, and crystal rims were analyzed following the techniques described in Schmitt et al. (2013) using the CAMECA ims 1270 and 1280-HR ion microprobes at University of California Los Angeles and Heidelberg University, respectively.

After SIMS analyses, zircon crystals were extracted from the indium mount, and analyzed for (U-Th)/He at Curtin University using analytical procedures detailed in Danišík et al. (2017a). In brief, zircon crystals were photographed and measured for dimensions in order to calculate alpha-ejection correction factors (also known as Ft-factors; Farley et al., 1996), and individually transferred into niobium microtubes. Radiogenic ^{4}He was extracted at ~1250 °C under ultra-high vacuum using a diode laser and analyzed on a Pfeiffer Prisma QMS-200 mass spectrometer. The released gas was purified using a hot (~350 °C) Ti-Zr getter, spiked with 99.9% pure ^{3}He and introduced into the mass spectrometer next to a cold Ti-Zr getter. ^{4}He/^{3}He ratios were measured using a channeltron detector operated in static mode and corrected for HD, ^{3}H and H_3 interferences by monitoring mass/charge = 1 u. A 're-extract' was run after each sample to verify complete outgassing of the crystals. He gas results were blank corrected by heating empty Nb tubes using the same procedure. Typically 10–15 blank analyses were measured before and after each crystal measurement.

After the ^{4}He measurements, microtubes containing the crystals were retrieved from the laser cell. Following the dissolution procedure (Evans et al., 2005), the samples were spiked with ^{235}U and ^{230}Th and dissolved in Parr bombs using HF, HNO_3 and HCl. Sample, blank and spiked standard solutions were analyzed for ^{238}U, ^{232}Th and ^{147}Sm on an Agilent 7500 ICP-MS at TSW Analytical Ltd (Perth). The total analytical uncertainty of uncorrected (U-Th)/He ages was calculated by propagating uncertainties of U, Th, Sm and He measurements. The uncorrected (U-Th)/He ages were corrected for ejection of alpha particles by applying Ft-correction factors

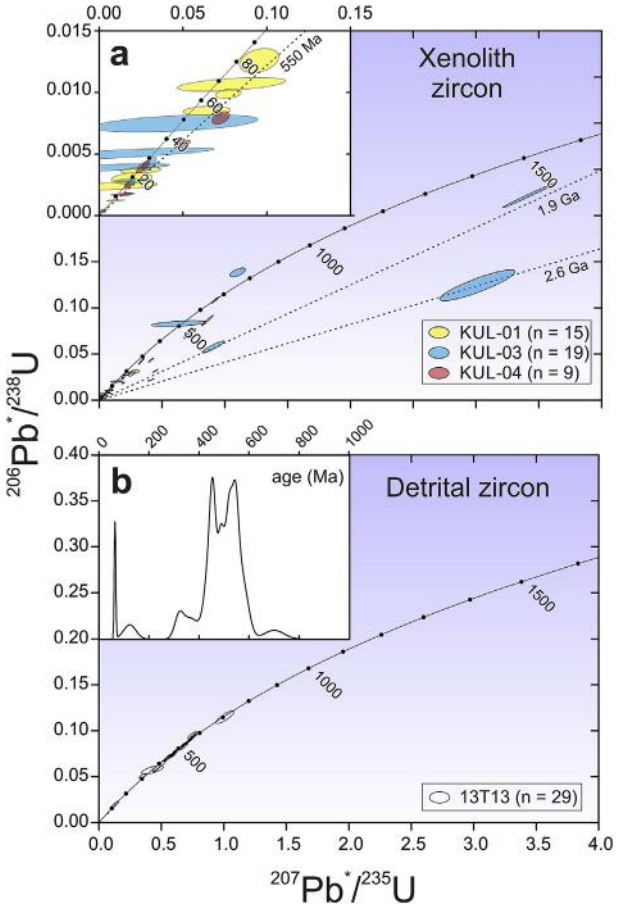

Fig. 8. Results of SIMS U-Pb zircon geochronology of pristine rims from **a)** pyrometamorphic metasedimentary xenoliths, and **b)** detrital zircon from local stream sand (sample 13T13, location UTM 35S 4276710 N 614780 E) with probability density curve of U-Pb ages in inset. Note young zircon rims and strong discordance in xenolith zircon crystals, which are lacking in the detrital population, indicating Pb-mobility due to pyrometamorphism probably facilitated by earlier metamictization. (For interpretation of the references to color in this figure legend, the reader is referred to the Web version of this article.)

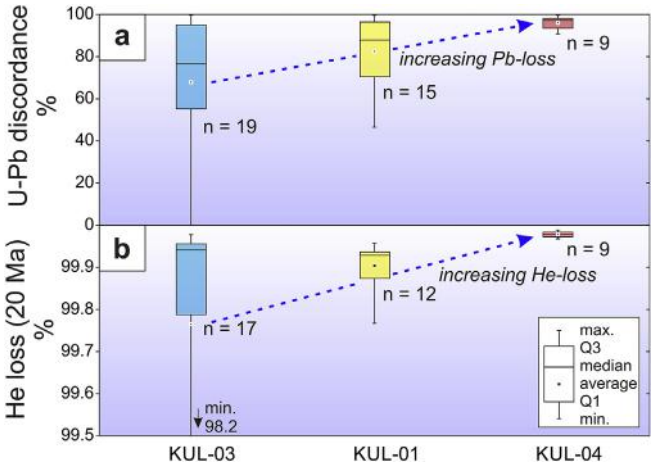

Fig. 9. Box plot of ZDD geochronology results for pyrometamorphic metasedimentary xenoliths showing **a)** U-Pb discordance and **b)** (U-Th)/He age expressed as percent He-loss relative to an estimated regional zircon cooling age of ca. 20 Ma (e.g., Gessner et al., 2001). Data show correlated Pb- and He-loss, indicating that zircon from sample KUL-04 experienced the highest degree of pre-eruptive ^{4}He degassing, and thus represents the best upper limit for the Çakallar eruption age from (U-Th)/He zircon dating. Discordance (D %) was calculated as: D (%) = (1 − R_x/R_y) × 100, with $R_x = {}^{238}U/{}^{206}Pb$ age, $R_y = {}^{207}Pb/{}^{206}Pb$ age when $^{207}Pb/^{206}Pb$ age >500 Ma, and R_y = 550 Ma (the main peak in the regional detrital zircon population) when $^{207}Pb/^{206}Pb$ age <500 Ma.

calculated after Farley et al. (1996) assuming a homogeneous distribution of U and Th. Given the difference between U-Pb and Ft-corrected (U-Th)/He ages exceeded 1 Ma, no correction for disequilibrium was applied to the Ft-corrected (U-Th)/He ages. The accuracy of the zircon (U-Th)/He dating procedure was monitored by replicate analyses of Fish Canyon Tuff zircon (n = 12) measured over the period of this study as internal standard, yielding a mean (U-Th)/He age of 28.2 ± 0.9 Ma (1σ), consistent with the reference (U-Th)/He age of 28.3 ± 1.3 Ma (Reiners, 2005). The eruption ages were averaged using Isoplot 4.15 (Ludwig, 2012), weighted by the assigned/internal errors option.

2.4. 3D stereo image modelling

One of the footprints from the collection of Hacettepe University was photographed from multiple positions at 15.1 megapixel resolution and modelled in three dimensions (Fig. 2a) using a multi-view stereophotogrammetry algorithm (SfM-MVS: Structure from Motion/Multi-view Stereo, Ullman, 1979; Lowe, 2004). Rock painting photographs were enhanced using a saturation stretching algorithm (Gillespie et al., 1986; Le Quellec et al., 2013) to reconstruct faded parts of the painting (Fig. 3c).

3. Geochronology results

We applied ZDD geochronology to Kula metasedimentary xenoliths from C2 scoria deposits, based on previous success in dating Quaternary felsic (Schmitt et al., 2012, 2014a, 2014b; Guillou et al., 2017; Danišík et al., 2012) and mafic eruptions (Blackburn et al., 2007; Schmitt et al., 2013). In parallel, we carried out cosmogenic surface exposure dating, which is well established for providing precise ages for surfaces of basaltic lava, and in favorable cases, pyroclastic blocks and bombs (e.g., Heineke et al., 2016; Zreda et al., 1993; Phillips, 2003; Dunbar and Phillips, 2004; Vazquez and Woolford, 2015). Three lava flow samples (KUL-08, KUL-09, KUL-10) yielded closely overlapping cosmogenic ^{36}Cl ages of 3.9 ± 0.9 ka, 5.3 ± 1.1 ka and 5.4 ± 1.2 ka (all errors stated at 1σ, Table 1; Fig. 7). One of the three bombs/blocks from the rim of the scoria cone (KUL-06) yielded a cosmogenic ^{36}Cl age of 4.7 ± 1.0 ka that agrees closely with the lava flow ages, whereas the ages from the other two bombs/blocks (KUL-05, KUL-07) are older: 7.5 ± 1.0 ka and 10.6 ± 1.9 ka (Table 1; Fig. 7).

Single crystal zircon (U-Th)/He ages of xenoliths KUL-01 and KUL-03 range from 3.8 to 51.2 ka (n = 16) and from 5.2 to 361 ka (n = 18), respectively. In contrast, sample KUL-04 shows a much narrower (U-Th)/He age distribution ranging from 3.4 to 10.9 ka (n = 10), with a weighted average age of 4.7 ± 0.7 ka and mean square of weighted deviates (MSWD) of 0.30, indicating at high confidence a single age population (Table 1; Supplementary Table 2; Fig. 7).

$^{238}U/^{206}Pb$ zircon rim ages for all xenolith samples are often discordant and variable with ranges of ca. 2.2–534 Ma (KUL-01), 1.8–1292 Ma (KUL-03), and 2.4–141 Ma (KUL-04), significantly predating the (U-Th)/He ages. Age discordance is highest in KUL-04 (91–99%), whereas many grains in KUL-01 and KUL-03 are concordant or show only moderate discordance (Fig. 8a). Detrital zircon weathered from local metasediments was analyzed for comparison (sample 13T13) and yielded generally concordant $^{238}U/^{206}Pb$ rim ages between 64 and 701 Ma; only one grain showed discordance of ca. 83% (Fig. 8b; Supplementary Table 3). For

many young (Cenozoic) ages, degrees of discordance are difficult to assess because of the comparatively large uncertainties of $^{235}U/^{207}Pb$ ages, but the relative scarcity of young rims in the detrital $^{238}U/^{206}Pb$ zircon age distribution compared to xenolith zircon rims underscores that zircon discordance and Pb-loss is a consequence of pyrometamorphism when xenoliths were heated by basaltic magma. Pb-diffusion is exceedingly slow in crystalline zircon even at magmatic temperatures (Cherniak and Watson, 2001). The observed significant Pb-loss from the outermost crystal rims during a brief heating interval therefore requires fast diffusion which is characteristic for metamict zircon (Cherniak and Watson, 2001).

4. Discussions and conclusions

4.1. Significance of ZDD and cosmogenic surface exposure age results

The thermal history of crustal xenoliths depends on the timing of entrapment into basaltic magma and subsequent eruptive cooling. Whereas eruptive cooling was equally rapid for all xenoliths sampled here because of their close proximity in the outcrop, the duration of pre-eruptive heating was likely different. There is also the possibility of thermal gradients within xenoliths of different sizes if the heating duration was brief, and variable He retentivity in zircon depending on accumulated radiation damage (Reiners, 2005; Hourigan et al., 2005; Blondes et al., 2007; Danišík et al., 2017b). However, xenolith clast-sizes were similar (5–10 cm in diameter), as expected for a well-sorted fall-out deposit. Given the high dispersion of (U-Th)/He ages and generally moderate degrees of U-Pb discordance (Figs. 7–9) we thus interpret samples KUL-01 and KUL-03 to have experienced brief heating and thus incomplete resetting of the (U-Th)/He system in many zircon crystals. By contrast, (U-Th)/He ages for KUL-04 form a tight cluster with a limited spread that can be solely attributed to analytical error (Figs. 8 and 9). This interpretation is supported by highly discordant U-Pb zircon rim ages for KUL-04, suggesting significant post-crystallization Pb-loss, and by proxy more efficient He-loss because of the higher diffusivity of He relative to Pb (Fig. 9) indicated by experimental diffusion data (Reiners et al., 2004). Based on these two independent strands of evidence for mobilization of He and Pb, we interpret KUL-04 as the xenolith with the most efficient heating that fully reset the (U-Th)/He system in all zircon crystals, and consequently its (U-Th)/He age of 4.7 ± 0.7 ka as being closest to the eruption age. Equally young, apparently fully reset zircon (U-Th)/He ages exist in samples KUL-01 and KUL-03 (Fig. 7: orange crosses; Supplementary Table 2), but the majority of zircon crystals in those samples retained small amounts of inherited ^{4}He.

Cosmogenic ^{36}Cl ages for the cone breaching basaltic lava flow (KUL-08, KUL-09, KUL-10) reproduced excellently, yielding a weighted average age of 4.7 ± 0.6 ka (Fig. 7). Our field data unequivocally indicate that cone construction and lava outflow were synchronous. Cosmogenic nuclide ages obtained on lava flow surfaces thus indirectly date burial of the hydrovolcanic ash surrounding the Çakallar cone (Fig. 5). Exposure ages for basaltic blocks/bombs (this study) and an accidental metasedimentary lithic clast (Heineke et al., 2016) from Çakallar pyroclastic deposits tend to predate cosmogenic ^{36}Cl ages for lava surface samples, with the exception of sample KUL-06, which is concordant with the lava ^{36}Cl ages. The discrepancy between older cosmogenic nuclide ages for (some) pyroclastic blocks/bombs and lithics on one hand, and younger cosmogenic nuclide ages for the lava flow and the (U-Th)/He ages of KUL-04 on the other hand can be resolved based on geologic observations: Firstly, field relations demonstrate coeval cone and lava flow formation, which rules out a temporal hiatus. Secondly, there is no evidence for significant erosion or burial of the basalt flow, and the exposure ages are therefore considered reliable estimates for the eruption age. Thirdly, the sample with the oldest cosmogenic ^{36}Cl age of 10.6 ± 1.3 ka (KUL-07) is from an ~40 cm diameter basalt block, which is distinctively rounded and denser than other Çakallar bombs. This strongly suggests that KUL-07 represents an accidental block, which was possibly derived from local older, now hidden, basaltic deposits (cf. Fig. 4; Kayan, 1992) or more likely from reworking of older deposits outcropping upstream Gediz River (Fig. 1). This could also be the case for sample KUL-05, although individual age uncertainties overlap with those of the lava samples. The ~20 cm diameter metasedimentary xenolith in Heineke et al. (2016) with an 11.2 ± 1.1 ka cosmogenic ^{10}Be age was also described as rounded. It was noted that the metasedimentary xenolith is more fine-grained than augen gneiss in the vicinity of Çakallar cone, and therefore argued for vertical transport within the magma conduit (Heineke et al., 2016). By the same token, the lithologic difference could also indicate lateral transport, which is consistent with abundant allochthonous gabbro and schist boulders in nearby streambeds. If these lithics are accidental detritus, they would have been exposed to cosmic radiation prior to eruption, and thus would yield erroneously old eruption ages. We therefore interpret the weighted average age from (U-Th)/He zircon and cosmogenic ^{36}Cl geochronology of 4.7 ± 0.5 ka as the currently most consistent eruption age constraint for Çakallar volcano, in agreement with the generally late Holocene age range determined for other β4 basaltic scoria cones and lava flows of Kula (Heineke et al., 2016 ; Fig. 7).

4.2. Bronze-age people witnessing the eruption

Kula footprints are one of only three examples in Anatolia where human ichnofossils are preserved, the other two being Barçın Höyük, northwest Anatolia (Özbal and Gerritsen, 2015) and Yenikapı harbor, İstanbul (Kızıltan and Polat, 2013). They are the only ones found in a volcanic context. Kula footprints on site and in museum collections are similar to modern human footprints on wet beach sand (Kayan, 1992). Their formation appears to be very similar to the Ka'u Desert footprints of Hawaii, which are also preserved in hydrovolcanic ash (Moniz-Nakamura, 2009). Although previous researchers have argued that the ash layer was wet due to rainfall during eruption (Barnaby, 1975; Tekkaya, 1976), raindrop impressions or rills are absent in the ash (Kayan, 1992; this study). We therefore argue for a hydrovolcanic eruption mechanism providing the humidity that generated sufficient coherence to preserve sharp prints in a wet pyroclastic surge deposit. The hypothesis that individuals were running away from the eruption (Barnaby, 1975) is dismissed based on footstep distances between 75 and 80 cm indicating normal walking speed rather than running (Yalçınlar, 1987; Kayan, 1992; Tekkaya, 1976; Akdeniz, 2011). Our observations confirm that the traces show a walking direction from west to east towards the Çakallar cone (Yalçınlar, 1987; Kayan, 1992). This may indicate a brief hiatus after ash deposition which was long enough for humans to approach the volcano after its initial outburst.

Despite their proximity, it currently remains unresolved whether there is a genetic link between the human footprints and the Kanlıtaş rock shelter painting (Akdeniz, 2011). Prehistoric petrographs and petroglyphs abound throughout Western Anatolia (e.g., Latmos-Aydın, Peschlow-Bindokat and Gerber, 2012; Konaklı-İzmir, Akdeniz, 2011; Çavdarhisar-Kütahya, Somuncuoğlu, 2007), but the cone-circle motive at Kanlıtaş (Fig. 3) appears to be unique. Although hand-like patterns (Fig. 3) are also common in petrographs at Late Neolithic to Early Chalcolithic Latmos sites within ~150 km distance from Kanlıtaş (Peschlow-Bindokat, 2006;

Peschlow-Bindokat and Gerber, 2012), this motive is not distinctive enough for correlation (Peschlow-Bindokat, pers. comm.).

The idea that prehistoric humans depicted volcanic eruptions as awe-inspiring natural events has been proposed for several sites worldwide (e.g., Hasandağ, Central Anatolia, Turkey, Mellaart, 1964 and discussion in Schmitt et al., 2014b; Chauvet-Pont d'Arc, Ardèche, France, Nomade et al., 2016; Porak volcano, Syunik, Armenia, Karakhanian et al., 2002). The Kanlıtaş rock painting shares some similarities with these other prehistoric art pieces, but Çakallar-Kanlıtaş is unique because of the close proximity (~2 km) between the painting and the volcano, and the preservation of footprints that indicates the humans witnessed the eruption. Weighing evidence from the volcanologically consistent details in the painting, we hypothesize that Bronze-age eye-witnesses of the eruption also generated the rock art. This link between the Kanlıtaş painting and the eruption remains, however, tentative until firm temporal constraints for the painting can be established.

Our new field observations and geochronological results demonstrate that the eruption of the basaltic ash which hosts human and animal ichnofossils is nearly 250 ka younger than originally proposed (Ozansoy, 1968), and ca. 5 ka younger than the most recently determined date (Heineke et al., 2016). Based on field observations and mapping, we reconstructed a series of events where an initial phreatomagmatic eruption from a vent location few 100 m southwest of the main cone ejected ash-. After deposition, humans slowly moved over the wet ash blanket towards the vent location. Volcanic activity subsequently progressed towards dry Strombolian activity with deposition of scoria burying the ash and preserving the footprints. Cone building, concomitant with effusive lava outpouring, proceeded and was plausibly witnessed by humans from a safe distance. The Kanlıtaş rock painting ~2 km from the footprints site is tentatively interpreted as depicting the erupting Çakallar cone and its associated lava flow, which makes it the only candidate for a Prehistoric depiction of a volcano for which human presence during the eruption can be unequivocally demonstrated.

Data availability

The authors declare that the data supporting the findings of this study are available within the article and the Supplementary files.

Competing interests

The authors declare no competing interests.

Author contributions

Conceived and designed the experiments: IU MAS AKS MD. Performed the experiments: MAS AKS MD IU. Analyzed the data: IU AKS MAS MD ES EG. Contributed reagents/materials/analysis tools: AKS MD MAS IU. Wrote the paper: IU MAS AKS MD ES EG. Fieldwork and sample collection: IU MAS AKS ES EG.

Acknowledgements

Authors acknowledge L. Akın for her help in zircon separation. We would like to thank E. Çubukçu for his constructive remarks and contribution to the fieldwork. We thank E. Aydın who was involved in 3D modelling of the footprint. Kula Geopark personnel Y. Karakuzu and A. Karataş are thanked for their contribution to fieldwork. R. Hetzel kindly provided a sand sample for detrital zircon extraction. An anonymous reviewer and S. Niedermann are thanked for their valuable reviews, and Janet C. Harvey and A.M.C. Şengör for their comments on an earlier version. Authors thank C. May and C. Scadding for solution ICP-MS analyses, and I. Dunkl for sharing PepiFLEX software for ICP-MS data reduction. M.D. was supported by the AuScope NCRIS2 program, Australian Scientific Instruments Pty Ltd., Australian Research Council (ARC)Discovery funding scheme (DP160102427) and Curtin Research Fellowship. Surface exposure dating of basalt samples was funded by Hacettepe University, Scientific Research Projects Coordination Unit, Project no: FDS-2016-9590. The ion microprobe facility at UCLA is partly supported by a grant from the Instrumentation and Facilities Program, Division of Earth Sciences, National Science Foundation. The HIP facility at Heidelberg University is operated under the auspices of the DFG Scientific Instrumentation and Information Technology program.

Appendix A. Supplementary data

Supplementary data to this article can be found online at https://doi.org/10.1016/j.quascirev.2019.03.030.

References

Akal, C., Bulut, S., Kaya, T.T., Savaşçın, M.Y., Süvari, E.F., Tare, A., 2009. Turkey offers a new geopark to the world: katakekaumene - Burnt Fires Geopark project. In: Neto de Carvalho, C., Rodrigues, J. (Eds.), Geotourism & Local Development, Idanha-A-Nova, pp. 138–148.

Akdeniz, E., 2011. Some evidence on the first known residents of Katakekaumene (Burned Lands). Mediterr. Archaeol. Archaeometry 11 (1), 69–74.

ASF DAAC, 2016. ALOS PALSAR_Radiometric_Terrain_Corrected_high_res; Includes Material © JAXA/METI 2006. https://doi.org/10.5067/Z97HFCNKR6VA. Accessed through ASF DAAC. https://www.asf.alaska.edu. (Accessed 5 March 2017).

Barnaby, W., 1975. International News 'picture story'. Nature 254, 553.

Blackburn, T.J., Stockli, D.F., Walker, J.D., 2007. Magnetite (U-Th)/He dating and its application to the geochronology of intermediate to mafic volcanic rocks. Earth Planet. Sci. Lett. 259, 360–371.

Blondes, M.S., Reiners, P.W., Edwards, B.R., Biscontini, A., 2007. Dating young basalt eruptions by (U-Th)/He on xenolithic zircons. Geology 35 (1), 17–20.

Bunbury, J.M., Hall, L., Anderson, G.J., Stannard, A., 2001. The determination of fault movement history from the interaction of local drainage with volcanic episodes. Geol. Mag. 138, 185–192.

Cherniak, D.J., Watson, E.B., 2001. Pb diffusion in zircon. Chem. Geol. 172 (1–2), 5–24.

Danišík, M., Shane, P., Schmitt, A.K., Hogg, A., Santos, G.M., Storm, S., Evans, N.J., Fifield, L.K., Lindsay, J.M., 2012. Re-anchoring the late Pleistocene tephrochronology of New Zealand based on concordant radiocarbon ages and combined $^{238}U/^{230}Th$ disequilibrium and (U–Th)/He zircon ages. Earth Planet. Sci. Lett. 349, 240–250.

Danišík, M., Schmitt, A.K., Stockli, D.F., Lovera, O.M., Dunkl, I., Evans, N.J., 2017a. Application of combined U-Th-disequilibrium/U-Pb and (U-Th)/He zircon dating to tephrochronology. Quat. Geochronol. 40, 23–32.

Danišík, M., McInnes, B.I., Kirkland, C.L., McDonald, B.J., Evans, N.J., Becker, T., 2017b. Seeing is believing: visualization of He distribution in zircon and implications for thermal history reconstruction on single crystals. Sci. Adv. 3 (2), e1601121.

Dunbar, N.W., Phillips, F.M., 2004. Cosmogenic ^{36}Cl ages of lava flows in the Zuni–Bandera volcanic field, northcentral New Mexico, U.S.A. New Mex. Bur. Geol. Min. Resour. Bull. 160, 309–317.

Eastwood, W.J., Leng, M.J., Roberts, N., Davis, B., 2007. Holocene climate change in the eastern Mediterranean region: a comparison of stable isotope and pollen data from Lake Gölhisar, southwest Turkey. J. Quat. Sci. 22 (4), 327–341.

Erinç, S., 1970. Kula ve Adala arası genç volkan reliefi. İstanbul Üniversitesi Coğrafya Enstitüsü Dergisi 9 (17), 7–32.

Evans, N.J., Byrne, J.P., Keegan, J.T., Dotter, L.E., 2005. Determination of uranium and thorium in zircon, apatite, and fluorite: application to laser (U-Th)/He thermochronology. J. Anal. Chem. 60, 1159–1165.

Fabryka-Martin, J.T., 1988. Production of Radionuclides in the Earth and Their Hydrogeologic Significance, with Emphasis on Chlorine-36 and Iodine-129. PhD Thesis. Univ. of Arizona, Tucson, USA.

Farley, K.A., Wolf, R.A., Silver, L.T., 1996. The effects of long alpha-stopping distances on (U-Th)/He ages. Geochem. Cosmochim. Acta 60, 4223–4229.

Gessner, K., Ring, U., Johnson, C., Hetzel, R., Passchier, C.W., Güngör, T., 2001. An active bivergent trolling-hinge detachment system: Central Menderes metamorphic core complex in western Turkey. Geology 29 (7), 611–614.

Gillespie, A.R., Kahle, A.B., Walker, R.E., 1986. Color enhancement of highly correlated images. I. Decorrelation and HSI contrast stretches. Remote Sens. Environ. 20 (3), 209–235.

Gosse, J.C., Phillips, F.M., 2001. Terrestrial in situ cosmogenic nuclides: theory and application. Quat. Sci. Rev. 20, 1475–1560.

Göksu, H.Y., 1977. Fosil Insan Ayak Izleri Taşıyan Volkanik Tabakaların Termolüminesans Özellikleri Ve Izlerin Tarihlendirilmesi. PhD Thesis. Middle East

Technical University, Dept. Physics, Ankara.
Göksu, H.Y., 1980. The TL age determination of fossil human footprints. In: Proceedings of the 18th International Symposium on Archaeometry and Archaeological Prospection, Bonn, vol. 10. Rheinland-Verlag GmbH, Köln, Archaeo-Physika, Band, pp. 455–462, 14-17 March 1978.
Guillou, H., Scao, V., Nomade, S., Platevoet, B., Blamart, D., 2017. De la justesse des âges K-Ar: Exemple de la datation de deux dômes trachytiques du Gölcük (Turquie). Quaternaire 28 (2), 141–148.
Gumus, E., 2014. Geoparks: Multidisciplinary Tools for the Protection and Management of Geoheritage in Turkey. Kula Volcanic Area (Manisa) and Camlidere Fossil Forest (Ankara) as Case Studies. PhD Thesis. Aegean University, Department of Geography, Mytilene, Greece.
Hamilton, W.J., Strickland, H.E., 1841. On the Geology of Western Part of Asia Minor, vol. I. Transactions of the Geol. Society of London, 2nd Ser., p. 81
Heineke, C., Niedermann, S., Hetzel, R., Akal, C., 2016. Surface exposure dating of Holocene basalt flows and cinder cones in the Kula volcanic field (Western Turkey) using cosmogenic ^{3}He and ^{10}Be. Quat. Geochronol. 34, 81–91.
Hourigan, J.K., Reiners, P.W., Brandon, M.W., 2005. U-Th zonation-dependent alpha-ejection in (U-Th)/He chronometry. Geochem. Cosmochim. Acta 69, 3349–3365.
Jones, M.D., Roberts, N.C., Leng, M.J., 2007. Quantifiying climatic change through the last glacial–interglacial transition based on lake isotope paleohydrology from central Turkey. Quat. Res. 67, 463–473.
Karakhanian, A., Djrbashian, R., Trifonov, V., Philip, H., Arakelian, S., Avagian, A., 2002. Holocene-historical volcanism and active faults as natural risk factors for Armenia and adjacent countries. J. Volcanol. Geotherm. Res. 113, 319–344.
Kayan, İ., 1992. Demirköprü baraj gölü batı kıyısında Çakallar volkanizması ve fosil insan ayak izleri. Ege Coğrafya Dergisi (Aegean Geographical Journal) 6, 1–32.
Kızıltan, Z., Polat, M.A., 2013. The Neolithic at Yenikapı, Marmaray Metro Project Rescue Excavations. In: Özdoğan, M., Başgelen, N., Kuniholm, P. (Eds.), The Neolithic in Turkey. New Excavations and New Research. Vol. 5: Northwestern Turkey and Istanbul. Arkeoloji ve Sanat Yayınları, İstanbul, pp. 113–165.
Le Quellec, J.-L., Harman, J., Defrasne, C., Duquesnoy, F., 2013. DStretch® et l'amélioration des images numériques: applications à l'archéologie des images rupestres. Les Cahiers de l'AARS 16, 177–198.
Lifton, N., Sato, T., Dunai, T.J., 2014. Scaling in situ cosmogenic nuclide production rates using analytical approximations to atmospheric cosmic-ray fluxes. Earth Planet. Sci. Lett. 386, 149–160.
Lockley, M., Roberts, G., Kim, J.Y., 2008. In the Footprints of Our Ancestors: An Overview of the Hominid Track Record. Ichnos 15, 106–125.
Lowe, D.G., 2004. Distinctive image features from scale-invariant Keypoints. Int. J. Comput. Vis. 60, 91–110.
Ludwig, K.R., 2012. User's Manual for Isoplot 3.75. A Geochronological Toolkit for Microsoft Excel, Berkeley, California.
Marrero, S.M., Phillips, F.M., Caffee, M.W., Gosse, J.C., 2016. CRONUS-Earth cosmogenic ^{36}Cl calibration. Quat. Geochronol. 31, 199–219.
Marty, D., Strasser, A., Meyer, C.A., 2009. Formation and Taphonomy of Human Footprints in Microbial Mats of Present-Day Tidal-flat Environments: Implications for the Study of Fossil Footprints. Ichnos 16, 127–142.
Mellaart, J., 1964. Earliest of Neolithic Cities: Delving Deep into the Neolithic Religion of Anatolian Chatal Huyuk, Part II-Shrines of the Vultures and the Veiled Goddess. Illustrated London News, pp. 194–197.
Moniz-Nakamura, J.J., 2009. Hominid footprints in recent volcanic ash: new interpretations from Hawaii Volcanoes National Park. Ichnos 16, 118–123.
NASA, 2008. MODIS 32-day Global Composite MOD09A1, Goodes.EUAS.2005225, Collection 3, the Global Land Cover Facility, vol. 225. University of Maryland, College Park, Maryland, p. 2005. Day.
Nomade, S., Genty, D., Sasco, R., Scao, V., Féruglio, V., Baffier, D., et al., 2016. A 36,000-Year-Old Volcanic Eruption Depicted in the Chauvet-Pont d'Arc Cave (Ardèche, France)? PLoS One 11 (1), e0146621.
Ozansoy, F., 1968. Türkiye Pleistosen fosil insan ayak izleri. Maden Tetkik ve Arama Enstitüsü Dergisi 72, 204–208.
Özbal, R., Gerritsen, F., 2015. Barçın Höyük Excavations: The 2014 Season in perspective. In: Steadman, S., McMahon, G. (Eds.), The Archaeology of Anatolia: Recent Discoveries (2011–2014), vol. I. Cambridge Scholars Publishing, Cambridge, pp. 26–45 ch. III.
Peschlow-Bindokat, A., 2006. Tarihöncesi İnsan Resimleri: Latmos Dağları'ndaki Prehistorik Kaya Resimleri. Vehbi Koç Foundation, Sadberk Hanım Müzesi , İstanbul, Publ, ISBN 975-6959-16-9, 120 pg.
Peschlow-Bindokat, A., Gerber, C., 2012. The Latmos-Beşparmak Mountains. Sites with Early Rock Paintings in Western Anatolia. In: Özdoğan, M., Başgelen, Nezih, Kuniholm, Peter (Eds.), The Neolithic in Turkey. New Excavations & New Research 4. Western Turkey. Arkeoloji ve Sanat Yayınları, İstanbul, pp. 67–115.
Phillips, F.M., 2003. Cosmogenic ^{36}Cl ages of Quaternary basalt flows in the Mojave Desert, California, USA. Geomorphology 53, 199–208.
Radt, S., 2004. Strabons Geographika, v. 3 Buch IX-XIII: Text und Übersetzung. Vandenhoeck & Ruprecht, Göttingen, 680+1 p of corrigenda.
Reiners, P.W., 2005. Zircon (U-Th)/He Thermochronometry. Rev. Mineral. Geochem. 58 (1), 151–179.
Reiners, P.W., Spell, T.L., Nicolescu, S., Zanetti, K.A., 2004. Zircon (U-Th)/He thermochronometry: He diffusion and comparisons with ^{40}Ar/^{39}Ar dating. Geochem. Cosmochim. Acta 68 (8), 1857–1887.
Robinson, S.A., Black, S., Sellwood, B.W., Valdes, P.J., 2006. A review of palaeoclimates and palaeoenvironments in the Levant and Eastern Mediterranean from 25,000 to 5000 years BP: setting the environmental background for the evolution of human civilisation. Quat. Sci. Rev. 25, 1517–1541.
Sanver, M., 1968. A paleomagnetic study of Quaternary volcanic rocks from Turkey. Phys. Earth Planet. In. 1, 403–421.
Sarıkaya, M.A., 2009. Late Quaternary Glaciation and Paleoclimate of Turkey Inferred from Cosmogenic ^{36}Cl Dating of Moraines and Glacier Modelling, Hydrology and Water Resources. University of Arizona, Tucson, AZ, p. 303.
Schimmelpfennig, I., Benedetti, L., Finkel, R., Pik, R., Blard, P.-H., Bourlès, D., Burnard, P., Williams, A., 2009. Sources of in-situ ^{36}Cl in basaltic rocks. Implications for calibration of production rates. Quat. Geochronol. 4, 441–461.
Schmitt, A.K., Martín, A., Stockli, D.F., Farley, K.A., Lovera, O.M., 2012. (U-Th)/He zircon and archaeological ages for a late prehistoric eruption in the Salton Trough (California, USA). Geology 41 (1), 7–10.
Schmitt, A.K., Martín, A., Weber, B., Stockli, D.F., Zou, H., Shen, C.C., 2013. Oceanic magmatism in sedimentary basins of the northern Gulf of California rift. Geol. Soc. Am. Bull. 125 (11–12), 1833–1850.
Schmitt, A.K., Danišík, M., Siebel, W., Elitok, Ö., Chang, Y.-W., Shen, C.-C., 2014a. Late Pleistocene zircon ages for intracaldera domes at Gölcük (Isparta, Turkey). J. Volcanol. Geotherm. Res. 286, 24–29.
Schmitt, A.K., Danišík, M., Aydar, E., Şen, E., Ulusoy, I., Lovera, O.M., 2014b. Identifying the Volcanic Eruption Depicted in a Neolithic Painting at Çatalhöyük, Central Anatolia, Turkey. PLoS One 9 (1), e84711.
Somuncuoğlu, S., 2007. Taştaki Türkler ve Bozkır Kavimleri, Atlas 177, 129–147.
Şen, E., 2002. Kula Bölgesi (Batı Anadolu, Türkiye) volkanizmasının volkanolojik-petrolojik gelişiminin incelenmesi. PhD Thesis (in Turkish). In: Fen Bilimleri Enstitüsü, Hacettepe Üniversitesi. Ankara, Türkiye, 269 pg.
Şen, E., Aydar, E., Bayhan, H., Gourgaud, A., 2014. Volcanological characteristics of alkaline basalt and pyroclastic deposits, Kula volcanoes, western Anatolia. (in Turkish). Yerbilimleri 35 (3), 219–252.
Tekkaya, I., 1976. İnsanlara ait fosil ayak izleri. Yeryuvarı ve İnsan 1/2, 8–10.
Ullman, S., 1979. The interpretation of structure from motion. Proc. R. Soc. Lond. B Biol. Sci. 203, 405–426.
Vazquez, J.A., Woolford, J.M., 2015. Late Pleistocene ages for the most recent volcanism and glacialpluvial deposits at Big Pine volcanic field, California, USA, from cosmogenic ^{36}Cl dating. Geochem. Geophys. Geosyst. 16, 2812–2828.
Washington, H.S., 1893. The Volcanoes of the Kula Basin in Lydia. PhD Thesis. University of Leipzig.
Westaway, R., Pringle, M., Yurtmen, S., Demir, T., Bridgland, D., Rowbotham, G., Maddy, D., 2004. Pliocene and Quaternary regional uplift in western Turkey: the Gediz River terrace staircase and the volcanism at Kula. Tectonophysics 391 (1–4), 121–169.
Westaway, R., Guillou, H., Yurtmen, S., Beck, A., Bridgland, D., Demir, T., Scaillet, S., Rowbotham, G., 2006. Late Cenozoic uplift of western Turkey: Improved dating of the Kula Quaternary volcanic field and numerical modelling of the Gediz River terrace staircase. Glob. Planet. Chang. 51 (3–4), 131–171.
Yalçınlar, İ., 1987. Gediz vadisinde prehistoric insanların ayak izleri. İstanbul Üniversitesi Coğrafya Dergisi 2, 71–80.
Zreda, M.G., Elmore, D., Phillips, F.M., Kubik, P.W., Sharma, P., 1993. Cosmogenic ^{36}Cl dating of a young basaltic eruption complex, Lathrop Wells, Nevada. Geology 21 (1), 57–60.